

# Supplementary Material

## Beyond Correlation Filters: Learning Continuous Convolution Operators for Visual Tracking

Martin Danelljan, Andreas Robinson, Fahad Shahbaz Khan, Michael Felsberg

CVL, Department of Electrical Engineering, Linköping University, Sweden  
{martin.danelljan, andreas.robinson, fahad.khan, michael.felsberg}@liu.se

In this supplementary material of [6] we provide additional derivations and implementation details. Section 1 provides details about the derivation of eq. (5) in the paper. Section 2 contains detailed derivations of the Fourier coefficients of the desired convolution output  $y_j$  and the interpolation functions  $b_d$ , described in section 3.4 in the paper. Details about the numerical optimization is given in section 3. We provide detailed results on the OTB-2015 and Temple-Color datasets in sections 4 and 5 respectively. In our object tracking experiments, we use the same parameter settings for our method in all state-of-the-art comparisons (sections 5.2, 5.3 and 5.4), i.e. for *all* datasets and videos. Further, we use the same parameter settings for all feature point tracking experiments. Code, raw result files and a video of qualitative feature point tracking results on the MPI Sintel dataset are available at the project webpage <http://www.cvl.isy.liu.se/research/objrec/visualtracking/conttrack/index.html>.

### 1 Fourier Coefficients of the Interpolated Feature Map

We first derive the expression for the Fourier coefficients of the interpolated feature map  $J_d\{x^d\}$ , which is used to prove eq. (5) in the paper. The interpolation operator  $J_d : \mathbb{R}^{N_d} \rightarrow L^2(T)$  for feature channel  $d$  is defined as (same as eq. (2) in the paper),

$$J_d\{x^d\}(t) = \sum_{n=0}^{N_d-1} x^d[n] b_d \left( t - \frac{T}{N_d} n \right). \quad (1)$$

Here,  $b_d \in L^2(T)$  is the interpolation function for channel  $d$ . From the shift property [21], it follows that  $b_d(t - \frac{T}{N_d}n)$  has Fourier coefficients  $\exp(-i\frac{2\pi}{N_d}k)\hat{b}_d[k]$ . By utilizing linearity, the Fourier coefficients of (1) are then derived as,

$$\widehat{J_d\{x^d\}}[k] = \sum_{n=0}^{N_d-1} x^d[n] e^{-i\frac{2\pi}{N_d}nk} \hat{b}_d[k] = \hat{b}_d[k] \sum_{n=0}^{N_d-1} x^d[n] e^{-i\frac{2\pi}{N_d}nk} = \hat{b}_d[k] X^d[k]. \quad (2)$$

Here,  $X^d[k] := \sum_{n=0}^{N_d-1} x^d[n] e^{-i\frac{2\pi}{N_d}nk}$ ,  $k \in \mathbb{Z}$  is the periodically extended discrete Fourier transform (DFT) of  $x^d$ . The Fourier coefficients of the confidence output (eq. (5) in the paper) are then derived from (2) here and eq. (1) in the paper by exploiting linearity and the first convolution property [21] (see section 3.1 in the paper) of the Fourier coefficients.

## 2 Fourier Coefficients of $y_j$ and $b_d$

We construct the desired convolution output  $y_j$  and interpolation function  $b_d$  as periodic repetitions of functions defined on the real line. For an integrable function  $g \in L^1(\mathbb{R})$ , we define the  $T$ -periodic repetition (or periodic summation) as  $g_T(t) = \sum_{n=-\infty}^{\infty} g(t - nT)$ . The Fourier coefficients  $\hat{g}_T[k]$  of  $g_T$  can then be obtained by evaluating the Fourier transform  $\hat{g}(\xi) = \int_{-\infty}^{\infty} g(t)e^{-i2\pi\xi t} dt$  of  $g$  at discrete locations using Poisson summation formula [21],

$$\hat{g}_T[k] = \frac{1}{T} \hat{g}\left(\frac{k}{T}\right). \quad (3)$$

In the proposed learning framework,  $y_j \in L^2(T)$  is the desired output of  $S_f\{x_j\}$ , i.e. the convolution operator applied to the sample  $x_j$ . Thus, in our formulation, the training sample  $x_j$  is labeled by an entire confidence function (or heat-map)  $y_j$  of the target presence at all continuous locations. The function value  $y_j(t)$  represents the labeled confidence score at the location  $t \in [0, T)$ . As  $y_j \in L^2(T)$  is arbitrary, it can be tailored for the specific application. For the visual tracking, a suitable approach is to construct  $y_j$  based on a Gaussian function. We let  $y_j(t) = \sum_{n=-\infty}^{\infty} z_j(t - nT)$  be the periodic repetition of the Gaussian function,

$$z_j(t) = e^{-\frac{1}{2\sigma^2}(t-u_j)^2}. \quad (4)$$

Here,  $u_j \in [0, T)$  is the estimated location of the target (or feature point) in the corresponding sample  $x_j$  and  $\sigma$  is a parameter. The Fourier transform of (4) is derived as  $\hat{z}_j(\xi) = \sqrt{2\pi\sigma^2} \exp(-i2\pi u_j \xi) \exp(-2\sigma^2(\pi\xi)^2)$  using the transform pair of a Gaussian function and the shift property (see e.g. [21]). The Fourier coefficients are thus computed using (3) as,

$$\hat{y}_j[k] = \frac{1}{T} \hat{z}_j\left(\frac{k}{T}\right) = \frac{\sqrt{2\pi\sigma^2}}{T} \exp\left(-2\sigma^2\left(\frac{\pi k}{T}\right)^2 - i\frac{2\pi}{T}u_j k\right). \quad (5)$$

The interpolation functions  $b_d$ , used in the interpolation operator (1), are constructed using the standard cubic spline kernel [24],

$$b(t) = \begin{cases} (a+2)|t|^3 - (a+3)t^2 + 1 & |t| \leq 1 \\ a|t|^3 - 5at^2 + 8a|t| - 4a & 1 < |t| \leq 2 \\ 0 & |t| > 2 \end{cases}. \quad (6)$$

In our experiments, we use the value  $a = -0.75$  for the shape parameter. The interpolation function for channel  $d$  is obtained by first rescaling  $b$  to the sample interval  $T/N_d$ . It is then shifted half an interval  $T/(2N_d)$  to align the origin of the continuous coordinate system with the sampling intervals of the feature map. The resulting interpolation kernel  $c_d$  and its Fourier transform are given by,

$$c_d(t) = b\left(\frac{N_d}{T}\left(t - \frac{T}{2N_d}\right)\right), \quad \hat{c}_d(\xi) = \frac{T}{N_d} e^{-i\pi\frac{T}{N_d}\xi\hat{b}}\left(\frac{T}{N_d}\xi\right) \quad (7)$$

Here,  $\hat{c}_d$  is obtained through the shift and scaling property of the Fourier transform. The analytical expression for the Fourier transform of (6) is given by,

$$\hat{b}(\xi) = \frac{6(1 - \cos 2\pi\xi) + 3a(1 - \cos 4\pi\xi) - (6 + 8a)\pi\xi \sin 2\pi\xi - 2a\pi\xi \sin 4\pi\xi}{4\xi^4\pi^4}. \quad (8)$$

The Fourier coefficients of  $b_d(t) = \sum_{-\infty}^{\infty} c_d(t - nT)$  are obtained through (3) as,

$$\hat{b}_d[k] = \frac{1}{T}\hat{c}_d\left(\frac{k}{T}\right) = \frac{1}{N_d}\exp\left(-i\frac{\pi}{N_d}k\right)\hat{b}\left(\frac{k}{N_d}\right). \quad (9)$$

### 3 Conjugate Gradient Optimization

For the target tracking application we employ the Conjugate Gradient (CG) method [20] to iteratively optimize the filter coefficients  $\hat{\mathbf{f}}$  by solving the normal equations (e.q. (8) in the paper),

$$(A^H\Gamma A + W^H W)\hat{\mathbf{f}} = A^H\Gamma\hat{\mathbf{y}}. \quad (10)$$

Here, the matrix  $A$  originates from the data term of the loss (e.q. (7) in the paper) and consists of one diagonal block per feature dimension  $d$  and training sample  $j$ . The diagonal matrix  $\Gamma$  contains the sample weights  $\alpha_j$ . The matrix  $W$  corresponds to a multi-channel convolution operation, where each channel  $d$  is convolved with the Fourier coefficients  $\hat{w}$  of the penalty function. The vector  $\hat{\mathbf{y}}$  is the concatenation of the Fourier coefficients of all label functions  $y_j$  (see section 3.3 in the paper for more details).

We perform 100 CG-iterations in the first frame to converge to a good initial estimate of the filter  $\hat{\mathbf{f}}$ . In the subsequent frames, we use 5 iterations per frame and initialize CG with the current filter (as computed in the previous frame). To further speed up the convergence, we initialize the previous search direction in CG to a forgetting factor times the final conjugate direction used in the previous frame. This forgetting factor is set to  $(1 - \lambda)^{10}$ , where  $\lambda$  is the learning rate of the tracker. The CG method is commonly used with a preconditioner to improve the condition number of the matrix and thereby the convergence rate of the solver. We employ an approximate diagonal preconditioner, which is computed as an efficient weighted running average of the training samples.

Our Conjugate Gradient optimization has a number of advantages compared to the Gauss-Seidel approach used in [3,4] regarding complexity and implementation. First, CG does not require explicit evaluations of the matrix product  $A^H\Gamma A$ . We therefore obtain a linear  $\mathcal{O}(D)$  instead of quadratic  $\mathcal{O}(D^2)$  complexity of the computations and memory consumption in the number of feature channels  $D$ . This is important for high-dimensional deep feature maps, as employed in this work. Secondly, CG can utilize the specific sparsity structure of the problem (10). We exploit that  $A$  can be permuted to a block-diagonal structure, containing one (dense) block matrix per Fourier coefficient  $k = -K, \dots, K$ .

The operations  $\mathbf{v} \mapsto A\mathbf{v}$  and  $\mathbf{v} \mapsto A^H\mathbf{v}$  in CG is implemented solely using dense block-wise matrix-vector multiplications. We also use the fact that the matrices  $W$  and  $W^H$  correspond to convolution operations over all feature channels with the kernel  $\hat{w}$  and its Hermitian adjoint respectively. The operation  $\mathbf{v} \mapsto W^H W\mathbf{v}$  in CG is performed as convolutions and thus  $W$  is not constructed explicitly. Since the Fourier coefficients of a real function obey the Hermitian symmetry, we only need to process half the Fourier coefficients  $0 \leq k \leq K$ . This effectively halves the computations and memory consumption of the training procedure. Finally, as the required operations in (10) are implemented as either block-wise dense matrix-vector multiplications, ordinary convolutions or element wise multiplications, our framework does not require explicit handling of sparse matrices (using e.g. sparse matrix libraries), which simplifies implementation.

## 4 Detailed Results on OTB-2015

In this supplementary material, detailed results on OTB-2015 [25] with 100 videos are provided. Videos and ground truth are available at <https://sites.google.com/site/benchmarkpami/>. Figure 1 contains the success plots for all 11 attributes and Table 2 shows the per-video overlap precision for all trackers in the comparison.

## 5 Detailed Results on Temple-Color

We also present detailed results on the Temple-Color dataset [17] with 128 videos. Videos and ground truth are available at <http://www.dabi.temple.edu/~hbling/data/TColor-128/TColor-128.html>. The per-video overlap precision for all trackers in our comparison are reported in table 2.

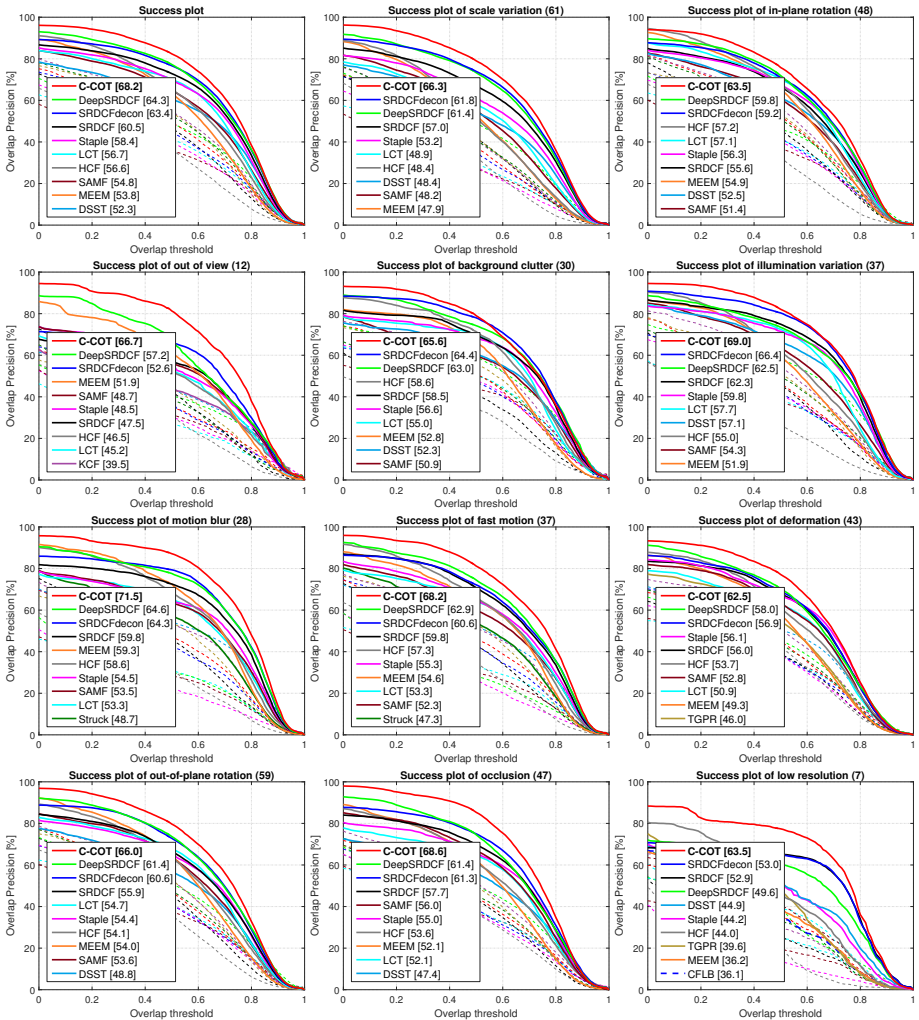


**Fig. 1.** Success plots on OTB-2015 [25] dataset. The overall success plot (top-left) is computed over the entire dataset (same as in figure 2a in the paper). We also show the success plots for all 11 attributes. The title of each attribute plot contains the name of the attribute and the number of videos associated with it. The area-under-the-curve (AUC) score is shown in the legend. For clarity, we only display the top 10 trackers in the legend. Our object tracking framework achieves the best results on all 11 attributes.

**Table 1.** A per-video comparison on the OTB-2015 dataset [25] with 100 videos. The results are shown in terms of overall precision (OP), in percent), which corresponds to the PASCAL criterion. The best and second best results for each video are shown in red and blue font respectively. Our object tracking framework achieves a significant gain of 5.1% in mean OP, compared to the second best tracker (DeepSRDCF).

Video	EDFT	LSHT	DFT	ASLA	LiD	Struck	CFILB	ACT	FCPR	KCF	DSST	SAMF	DAT	MEMM	LCT	HCF	Staple	SRDCF	SRDCF+decon	DeepSRDCF	C-COT
	[3]	[12]	[23]	[14]	[11]	[15]	[9]	[7]	[10]	[13]	[2]	[6]	[20]	[26]	[29]	[18]	[8]	[5]	[4]	[28]	[16]
Basketball	31	4.55	71.6	65.2	31.3	11	9.1	48.7	91.3	89.8	69.8	96.7	80.5	83	<b>99.9</b>	<b>99.9</b>	87.2	41.2	30.1	28.3	98.9
Biker	26.7	8.89	26.7	46.7	32.6	26.7	46.7	<b>87.4</b>	26.7	28.1	31.9	44.1	25.9	26.7	46.7	46.7	46.7	46.7	46.7	54.9	<b>53.9</b>
Bir1	26.7	4.41	26.2	24.5	0.49	15.4	0.98	2.45	<b>31.1</b>	6.37	6.62	5.64	<b>30.7</b>	4.41	<b>31.1</b>	91.9	27.7	6.37	5.64	26.2	5.64
Bir2	94.9	85.9	71.7	50.5	4.2	52.5	47.5	<b>99.9</b>	85.9	46.5	25.5	<b>99.9</b>	<b>99.9</b>	77.5	<b>99.9</b>	96	54.5	54.5	54.5	83.8	100
BirBody	11.7	29.1	11.5	44	98.8	41.3	53.9	98.5	58.7	62.3	95.8	37.1	98.8	90.4	<b>99.7</b>	<b>100</b>	<b>99.7</b>	69.5	<b>99.9</b>	<b>99.9</b>	<b>99.9</b>
BirCar1	1.48	1.21	7.68	2.29	13.6	<b>99.9</b>	50.4	69.9	94.5	<b>100</b>	98.8	1.48	<b>100</b>	<b>100</b>	<b>100</b>	<b>100</b>	<b>100</b>	<b>100</b>	<b>100</b>	<b>100</b>	<b>100</b>
BirCar2	7.35	21.9	17.4	12.3	84.8	93.8	94.7	94.7	93.8	94.7	<b>100</b>	<b>99.8</b>	48.7	94.7	<b>100</b>	<b>100</b>	<b>100</b>	<b>100</b>	<b>100</b>	<b>100</b>	<b>100</b>
BirCar3	5.6	30.8	11.8	12	93.6	<b>100</b>	56	32.8	93.3	<b>99.4</b>	<b>100</b>	<b>100</b>	<b>25.2</b>	<b>100</b>	<b>100</b>	<b>100</b>	<b>100</b>	<b>100</b>	<b>100</b>	<b>100</b>	<b>100</b>
BirCar4	96.8	33.7	<b>100</b>	21.8	42.6	<b>100</b>	<b>100</b>	<b>100</b>	<b>99.7</b>	<b>100</b>	<b>100</b>	<b>100</b>	<b>100</b>	<b>100</b>	<b>100</b>	<b>100</b>	<b>100</b>	<b>100</b>	<b>100</b>	<b>100</b>	<b>100</b>
BirFace	24.1	11.8	29	15	<b>100</b>	<b>100</b>	43	31.4	<b>100</b>	<b>100</b>	<b>100</b>	<b>100</b>	<b>28.9</b>	<b>100</b>	<b>100</b>	<b>100</b>	<b>100</b>	<b>100</b>	<b>100</b>	<b>100</b>	<b>100</b>
BirDwl	4.28	9.83	10.8	11.4	63.9	98.6	94.1	20.8	13.6	22.8	22	23.1	<b>99.8</b>	99	98.4	95.5	50.6	98.6	97.1	<b>100</b>	<b>100</b>
Board	19.4	86.5	19.9	50.9	14.1	79.9	68.1	73.4	11.3	85.5	84.2	<b>97.1</b>	20.1	82.5	85.4	94.7	77.8	85.7	95.7	96.6	87.2
Boh	1.71	32.6	4	1.43	17.7	2.99	<b>100</b>	1.43	94.3	<b>100</b>	<b>99.7</b>	96	88	98.9	98	99.7	1.43	1.43	1.43	74.6	90.6
Boh2	0.683	32.9	0.683	0.683	4.44	34.5	27	0.683	0.683	1.92	0.683	63.5	0.683	0.683	<b>88.4</b>	<b>99.1</b>	1.92	1.92	1.92	85.3	65.5
Box	16	33.7	30.0	57.0	61.6	88.7	32.1	35.6	5.8	35.7	36.6	42.7	5.8	38.7	98.6	53.7	41.5	41.5	46	30	89.5
Boy	98	50.7	88.3	43.5	82.9	97.5	98.5	95	99.2	<b>100</b>	<b>100</b>	<b>100</b>	96.3	96.2	<b>100</b>	<b>100</b>	<b>100</b>	<b>100</b>	<b>100</b>	<b>100</b>	<b>100</b>
Car	5.39	5.39	5.39	81.6	38.7	5.39	6.27	5.39	7.75	5.39	60.5	36.3	5.39	5.39	20.8	5.39	76.5	<b>100</b>	<b>100</b>	<b>100</b>	<b>100</b>
Car2	<b>100</b>	98.2	13.4	<b>100</b>	<b>100</b>	<b>100</b>	<b>99.7</b>	<b>100</b>	9.2	<b>100</b>	<b>100</b>	<b>100</b>	7.34	<b>100</b>	<b>100</b>	<b>100</b>	<b>100</b>	<b>100</b>	<b>100</b>	<b>100</b>	<b>100</b>
Car24	17.3	17.2	7.19	<b>100</b>	<b>99</b>	17	17.3	17.3	18.3	17.3	17.3	15.7	16.4	17.2	85.3	17.3	17.3	17.3	17.3	100	<b>100</b>
Car3	27.4	27.4	28.8	10.7	10.7	10.7	10.7	10.7	10.7	10.7	10.7	10.7	10.7	10.7	10.7	10.7	10.7	10.7	10.7	10.7	10.7
CarDark	68.3	60.6	33.6	<b>100</b>	<b>53.7</b>	<b>100</b>	<b>97.7</b>	<b>100</b>	69.2	<b>100</b>	69.2	10.3	20.4	<b>100</b>	<b>100</b>	<b>100</b>	<b>100</b>	<b>100</b>	<b>100</b>	<b>100</b>	<b>100</b>
CarScale	44.8	44.8	44.8	71	68.7	43.3	44.8	40.5	44.4	84.5	59.9	44.1	44.8	79	44.4	84.1	83.9	81	80.2	81	80.2
CliffBar	29.7	28.2	23.9	37.7	42.2	21.6	25.6	31.8	9.32	30.1	<b>88.6</b>	25.6	29.4	60.6	70.7	41.7	58.9	44.1	85	59.1	71.2
Color	11.4	49.8	8.59	14.4	57.4	<b>99.7</b>	70.4	64.3	88	72.2	85.2	79.7	47.8	95.5	91.4	91.4	77	63.6	65.6	50.5	54
Conc	92.1	92.8	57	22	100	100	100	100	100	100	100	100	100	100	100	100	100	100	100	100	100
Cousson	<b>100</b>	<b>100</b>	<b>100</b>	<b>100</b>	<b>100</b>	<b>100</b>	<b>100</b>	<b>100</b>	37.9	<b>100</b>	<b>100</b>	<b>100</b>	<b>99.7</b>	<b>100</b>	<b>100</b>	<b>100</b>	<b>100</b>	<b>100</b>	<b>100</b>	<b>100</b>	<b>100</b>
Crossing	75	40	64.2	<b>100</b>	45.8	95.8	<b>98.3</b>	88.3	98.3	95	<b>100</b>	<b>100</b>	<b>99.7</b>	<b>98.3</b>	<b>100</b>	95	<b>100</b>	<b>100</b>	<b>100</b>	<b>100</b>	<b>100</b>
Crowds	91	54.3	91	89	89	68.2	90.8	96.8	86.7	<b>100</b>	90.2	<b>99.7</b>	1.73	83.8	96.2	99.4	95.1	89.6	90.8	<b>100</b>	<b>100</b>
Dancer	89.3	88.4	89.8	<b>100</b>	88.9	85.8	88.3	90.7	<b>97.6</b>	<b>97.6</b>	<b>100</b>	73.8	80.9	<b>100</b>	<b>97.6</b>	<b>100</b>	<b>100</b>	<b>100</b>	<b>100</b>	<b>100</b>	<b>100</b>
Dance2	<b>100</b>	<b>100</b>	<b>100</b>	<b>100</b>	<b>100</b>	<b>100</b>	<b>100</b>	<b>100</b>	<b>100</b>	<b>100</b>	<b>100</b>	<b>100</b>	<b>100</b>	<b>100</b>	<b>100</b>	<b>100</b>	<b>100</b>	<b>100</b>	<b>100</b>	<b>100</b>	<b>100</b>
David	55.4	28.2	23.4	91.9	61.1	23.6	23.6	82.6	80.5	62.2	<b>100</b>	95.8	39.1	62.6	92.8	60.1	96.2	95.9	97.5	<b>100</b>	<b>100</b>
David2	<b>100</b>	<b>100</b>	54.2	83.6	<b>100</b>	<b>100</b>	<b>100</b>	<b>100</b>	<b>100</b>	<b>100</b>	<b>100</b>	<b>100</b>	<b>100</b>	<b>100</b>	<b>100</b>	<b>99.2</b>	<b>100</b>	<b>100</b>	<b>100</b>	<b>100</b>	<b>100</b>
David3	87.3	74.6	74.2	49.6	32.1	33.7	53.6	87.7	98.8	99.2	52.8	<b>100</b>	<b>100</b>	94	98	<b>100</b>	<b>100</b>	<b>100</b>	<b>100</b>	<b>100</b>	<b>100</b>
Deer	63.4	4.23	31	4.23	28.2	100	<b>100</b>	81.7	78.9	88.7	98.6	<b>100</b>	81.7	83.1	83.1	83.1	83.1	83.1	83.1	83.1	83.1
Diving	18	16	18.6	18.6	18.6	18.6	18.6	18.6	18.6	18.6	18.6	18.6	18.6	18.6	18.6	18.6	18.6	18.6	18.6	18.6	18.6
Dog	19.7	15	19.7	66.1	72.4	15.7	13.4	13.4	22.8	11.2	60.6	47.2	18.1	14.2	33.9	83.4	59.8	49.6	59.8	<b>79.5</b>	<b>83.5</b>
Dog1	64.4	54.3	52.1	89.9	75.6	65.2	58.4	65.3	66.9	65.1	<b>100</b>	72.8	65.2	62.9	<b>100</b>	65.2	<b>100</b>	<b>100</b>	<b>100</b>	<b>100</b>	<b>100</b>
Doll	49.3	23	35	92.2	69.3	68.9	72.4	49.6	86.4	55.2	<b>99.7</b>	65.2	18.3	72.9	99.4	72.9	99.9	<b>99.7</b>	<b>99.7</b>	90.1	<b>99.7</b>
DragonBall	22.1	19.5	11.5	13.9	15.3	8.85	61.9	23	38.1	30.1	61.9	63.7	38.8	80.5	31	78.8	58.4	30.1	22.1	85	<b>96.5</b>
Drunk	82.7	89.9	80.1	90.5	67	98.1	95.5	96.1	94.6	97.6	98.1	98.2	18.1	93.1	90.9	99.9	67.3	99.2	97.4	97.4	97.4
FaceOcc1	67.2	79.4	80.3	27.2	56.4	<b>100</b>	<b>98.8</b>	<b>100</b>	96.2	<b>100</b>	<b>100</b>	<b>100</b>	<b>100</b>	<b>100</b>	<b>100</b>	<b>100</b>	<b>100</b>	<b>100</b>	<b>100</b>	<b>100</b>	<b>100</b>
FaceOcc2	99.4	<b>99.8</b>	99.5	<b>100</b>	78.9	<b>100</b>	97.8	62.4	93.5	99.6	<b>100</b>	98.6	11.1	91.9	<b>99.8</b>	<b>100</b>	99.6	93.6	90.4	61.7	95.3
Fish	<b>100</b>	<b>100</b>	<b>86.4</b>	<b>100</b>	<b>100</b>	<b>100</b>	<b>100</b>	4.83	39.9	<b>100</b>	<b>100</b>	<b>100</b>	5.67	16.8	<b>100</b>	<b>100</b>	<b>100</b>	<b>100</b>	<b>100</b>	<b>100</b>	<b>100</b>
FootFace	54.7	65.5	55.6	64.5	44.1	78.7	57.3	58.7	64.2	66.9	66.5	70.3	52.3	77.8	<b>94.3</b>	61.7	66.3	67.8	76	74.5	74.5
Football	97.5	77.3	84.3	77.1	49	89.8	68	63.8	98.3	70.2	79	78.5	97.6	95.6	<b>100</b>	<b>100</b>	78.7	87.8	95.5	79	79
Football1	<b>100</b>	<b>100</b>	<b>100</b>	43.2	36.5	32.4	32.4	40.5	68.9	94.6	39.2	35.1	79.7	90.7	<b>100</b>	<b>100</b>	95.9	39.2	39.2	39.2	37.8
Freeman1	12.6	18.4	17.8	32.8	23.3	20.2	14.7	13.8	22.7	16.3	35.3	28.2	19	22.1	<b>65.3</b>	<b>29.8</b>	<b>86.5</b>	62.6	53.1	54.3	43.6
Freeman3	28.9	15.7	33	<b>91.7</b>	64.6	17.6	31.3	33	1.09	27.8	31.3	26.1	30.7	33	31.1	29.6	31.3	55.9	70.4	100	100
Freeman4	17	20.1	18	21.6	18.7	15.9	17.3	19.1	18.4	41.7	16.6	23.7	28.3	41.3	45.9	45.2	<b>87.6</b>	<b>90.5</b>	79.5	74.6	74.6
Football2	88	14	25.2	88	72.6	38.7	38.7	18.1	74.2	30.5	10.2	30.5	10.2	30.5	10.2	30.5	10.2	30.5	10.2	30.5	10.2
Girl2	71.3	81.3	71.3	71.3	71.3	71.3	71.3	71.3	71.3	71.3	71.3	71.3	71.3	71.3	71.3	71.3	71.3	71.3	71.3	71.3	71.3
Gym	7.04	31.2	6.91	4.95	35.6	11.1	31.3	26.9	35.5	34.3	1.56	35.1	29.3	37.9	23.5	40.8	<b>74.3</b>	<b>53.5</b>	<b>41.3</b>	35.5	61.3
Human2	30.1	16.8	9.13	93.2	48.8	71.5	54.4	17.6	19.5	18.3	55.8	56.9	29	83.4	94.4	80.4	95.5	94.9	94.2	94.2	94.2
Human3	0.53	1.24	0.53	0.648	0.53	1.06	0.53	0.53	0.471	0.471	2.77	0.471	67.7	65.8	80.4	32.4	3	3.18	77.9	39	<b>81.8</b>
Human4	19.3	19	18.7	19.3	13.6	21.1	19.5	19.5	53.5												

**Table 2.** A per-video comparison in the Temple-Coffee dataset [17] with 128 videos. The results are shown in terms of overlap precision (OP) in percent, which corresponds to the PASCAL criterion. The best and second best results for each video are shown in red and blue font respectively. Our approach achieves a significant gain of 4.6% in mean OP, compared to the second best tracker (SRDCFdecon).

Video	DPPT	SFMT	DPPT	DPPT	ASLA	LLD	Strack	CPLE	ACT	TOPK	KCF	SRST	SAMP	DAT	MEMB	LCF	RCF	Scale	SHPC	SRDCFdecon	DeepSRDCF	CCOT	
Airport	38.5	28.4	40.6	44.6	43.9	41.9	1.35	40.5	42.6	42.6	47.3	43.2	42.6	41.7	42.6	42.6	59	85.1	45.4	44.4	44.6	44.6	
Baby	29.7	18.2	29.7	30.9	61.5	27.4	29.7	29.7	32.1	27.4	39.7	39.2	29.7	27	29.1	29.1	36.3	90.9	38.3	35.9	38.3	38.3	
Beach01	12.8	12.8	12.8	12.8	12.8	12.8	12.8	12.8	12.8	12.8	12.8	12.8	12.8	12.8	12.8	12.8	12.8	12.8	12.8	12.8	12.8	12.8	
Beach02	1.09	0.142	4.26	2.06	3.55	8.4	59.4	49.6	85.7	93.6	11.8	8.6	88.4	68.5	80.6	82.7	83.9	65.2	78.3	54.9	89.2	89.2	
Ball	2.3	1.28	2.3	2.36	1.28	6.91	2.96	1.53	2.3	1.53	1.28	1.79	11.8	26.7	1.28	28.6	2.3	1.28	51.2	1.28	1.28	2.05	2.05
Ball2	0.94	0.964	1.13	2.04	1.04	0.345	0.173	4.2	40.4	39.1	40.4	44.2	67.2	33	54.1	37	61.4	37.5	91.5	83.1	90.4	90.4	
Ball3	69.3	29.2	69.3	59	84.4	8.8	68.4	61.3	69.3	56.1	69.3	69.3	69.3	69.3	69.3	69.3	69.3	69.3	69.3	69.3	69.3	69.3	
Ball4	1.09	1.09	4.83	0.372	2.37	2.42	0.372	4.83	1.3	1.21	1.3	4.05	4.69	3.35	6.79	4.09	4.09	4.09	4.09	4.09	4.09	4.09	
Ball5	31	43	29.1	37.3	43.1	81.9	28.8	43.1	43.1	21	43.1	43.1	43.1	43.1	43.1	43.1	43.1	43.1	43.1	43.1	43.1	43.1	
Ball6	11.7	10.5	12.1	11.5	7.49	11.9	11.1	14.3	9.68	19	16.7	34.7	11.1	15.3	19.4	33.3	56.9	67.3	48.5	48.5	73.2	73.2	
Beach03	6.59	12.1	7.01	13.2	10.1	36.5	37.3	10.1	10.8	13.9	16.5	38	88.2	3.75	37	33.2	39.7	35.1	27.1	42.1	42.1	42.1	
Beach04	9.4	9.1	9.3	9.2	4.76	9.1	59.9	9.75	64.8	99.8	34.7	76.9	72.3	94.1	59	79.4	71.4	82.8	87.5	64.8	97.1	97.1	
Beach05	37.8	78.9	14.4	38.9	98.9	83.3	37.8	43.1	91.1	20	36.7	22.2	89.5	54.4	28.9	28.9	85.6	43.3	97.8	41.1	47.8	47.8	
Bicycle	25.8	34.4	21	39.8	24.7	30.6	19.9	20.1	35.4	38.9	40.8	78.6	42.2	84.8	19.2	34.6	96.6	76.8	94.8	78.8	78.8	78.8	
Bill	14.4	4.2	79.5	9.1	12.9	71.9	11.5	74.3	9.1	76.7	99.7	100	74.2	54.7	76.7	76.7	100	100	100	100	100	100	
Bill2	2.34	2.34	2.34	14.8	15.8	2.34	2.34	2.34	2.34	2.34	13.5	10.1	2.34	2.34	2.34	9.98	13.8	53.8	99.7	90.4	85.2	85.2	
Bill3	19	19	19	32	26.1	21.8	19	19	41	61.1	19	19.9	93.9	19	19	19	19	19	19	19	19	19	
Bikeshow	2.72	2.92	4.9	3.05	1.39	8.77	12.7	15.3	2.65	21.6	7.48	35.7	70.7	4.6	2.22	96.2	11.5	22.4	19.4	22.4	63.1	63.1	
Box	94.9	6.2	94.9	9.09	43.1	40.5	17.5	99	57.6	51.5	52.5	35.6	39	38	16.8	38	85.9	37.6	65.1	96	100	100	
Box2	1.09	1.09	1.09	1.09	1.09	1.09	1.09	1.09	1.09	1.09	1.09	1.09	1.09	1.09	1.09	1.09	1.09	1.09	1.09	1.09	1.09	1.09	
Box3	5.04	5.04	5.04	6.1	16.2	5.04	5.04	5.04	5.04	5.04	5.7	39.3	4.51	5.04	5.04	5.04	5.04	5.04	5.04	5.04	5.04	5.04	
Box4	12.8	12.8	12.8	12.8	12.8	12.8	12.8	12.8	12.8	12.8	12.8	12.8	12.8	12.8	12.8	12.8	12.8	12.8	12.8	12.8	12.8	12.8	
Box5	11.7	11.4	1.4	1.43	17.7	1.43	2.25	100	2.29	54.3	100	97.7	36	88	95.6	38	100	1.43	1.43	1.43	74.8	90.6	
Box6	38	42.5	48.3	43.9	96.5	97.5	98.5	95	95.5	99.2	100	96.3	99.2	99	99	100	100	100	100	100	100	100	
Boulevard	10.8	10.8	10.8	10.8	10.8	10.8	10.8	10.8	10.8	10.8	10.8	10.8	10.8	10.8	10.8	10.8	10.8	10.8	10.8	10.8	10.8	10.8	
Car	24.6	34.7	24.6	24.1	33.9	29.1	31.9	20.1	30.1	37.8	32.4	23.8	93.9	98.7	88.1	90.4	88.1	97.5	96.7	96.7	96.7	96.7	
Car2	68.4	50.1	35.6	100	27.5	100	38.7	100	100	69.2	100	58.3	21.04	100	97.7	87.3	100	100	100	100	100	100	
Car3	44.8	44.8	44.8	44.8	44.8	44.8	44.8	44.8	44.8	44.8	44.8	44.8	44.8	44.8	44.8	44.8	44.8	44.8	44.8	44.8	44.8	44.8	
Car4	28.1	28.1	28.1	28.1	28.1	28.1	28.1	28.1	28.1	28.1	28.1	28.1	28.1	28.1	28.1	28.1	28.1	28.1	28.1	28.1	28.1	28.1	
Car5	99.3	99.3	100	100	74	98.8	100	97.4	97.1	71.6	96.6	84.8	86.6	84.8	86.6	84.8	86.6	84.8	86.6	84.8	99.3	99.3	
Car6	6.35	6.35	6.35	6.35	6.35	6.35	6.35	6.35	6.35	6.35	6.35	6.35	6.35	6.35	6.35	6.35	6.35	6.35	6.35	6.35	6.35	6.35	
Champ	17.1	28.9	18.1	22.1	50.3	19.1	13.1	36.6	30.5	19.5	79.5	56.1	41.9	22.1	29.5	29.5	30.9	83.2	71.8	71.8	78.2	78.2	
Chair	14.4	14.4	14.4	14.4	14.4	14.4	14.4	14.4	14.4	14.4	14.4	14.4	14.4	14.4	14.4	14.4	14.4	14.4	14.4	14.4	14.4	14.4	
Charger	21.4	10.7	8.97	10.7	49.1	60.7	61.6	10.7	10.7	24.3	10.7	45.7	61.6	75.7	59	71.3	67.9	92.7	94.8	77.9	72.1	72.1	
Crossing	75	11.7	64.2	100	45.8	95.8	98.7	88.3	98.7	95	100	100	97.5	80.3	96.7	96	100	100	100	100	100	100	
Exp	100	100	100	100	100	100	100	100	100	100	100	100	100	100	100	100	100	100	100	100	100	100	
Exp2	1.48	1.48	1.18	1.18	2.06	1.18	1.18	1.18	1.18	1.18	1.18	1.18	1.18	1.18	1.18	1.18	1.48	1.48	1.48	1.48	1.18	1.18	
Exp3	55.4	43.7	22.4	95.1	91.1	24	23.5	62.6	62.6	62.2	100	95.8	30.1	62.6	62.6	60.1	96.2	98.7	99.9	100	100	100	
Exp4	32.3	32.3	32.3	32.3	32.3	32.3	32.3	32.3	32.3	32.3	32.3	32.3	32.3	32.3	32.3	32.3	32.3	32.3	32.3	32.3	32.3	32.3	
Exp5	63.4	4.23	31	4.23	78.9	100	100	100	100	81.7	84.5	88.7	9.86	100	61.6	100	100	100	100	100	100	100	
Exp6	19	18.2	21.2	29	16.5	21.2	29	20.5	14.3	20.5	18.8	17.7	20.2	18.2	20.3	28.6	18.8	22.1	21.1	24.7	18.6	18.6	
Exp7	49.3	49.3	49.3	49.3	49.3	49.3	49.3	49.3	49.3	49.3	49.3	49.3	49.3	49.3	49.3	49.3	49.3	49.3	49.3	49.3	49.3	49.3	
Exp8	20.5	11.6	21.3	38.4	36.6	28.6	33	35.7	45.5	2.68	2.68	2.68	18.8	85.7	2.68	7.1	21.1	29.5	16.1	25	5.36	5.36	
Exp9	12.8	12.8	12.8	12.8	12.8	12.8	12.8	12.8	12.8	12.8	12.8	12.8	12.8	12.8	12.8	12.8	12.8	12.8	12.8	12.8	12.8	12.8	
Exp10	67.2	100	80.3	29	51.1	100	95.7	100	100	100	100	100	100	100	100	100	100	100	100	100	100	100	
Exp11	3.71	3.55	3.71	4.39	43.9	3.06	3.06	3.89	3.71	4.35	4.35	4.35	3.23	3.55	3.71	3.71	4.35	4.32	80	79.8	78.9	78.9	
Exp12	30.1	30.1	30.1	30.1	30.1	30.1	30.1	30.1	30.1	30.1	30.1	30.1	30.1	30.1	30.1	30.1	30.1	30.1	30.1	30.1	30.1	30.1	
Exp13	4.99	5.49	5.24	5.24	6.73	29.7	2.74	6.58	6.73	4.24	4.99	32.7	65.6	58.9	59.9	61.1	65.6	17.7	11.5	20.4	43.1	43.1	
Exp14	15.2	15.2	15.2	15.2	15.2	15.2	15.2	15.2	15.2	15.2	15.2	15.2	15.2	15.2	15.2	15.2	15.2	15.2	15.2	15.2	15.2	15.2	
Exp15	100	100	100	100	100	100	100	100	100	100	100	100	100	100	100	100	100	100	100	100	100	100	
Exp16	48.6	37	29.2	29.4	29.4	80.2	96.8	36.4	83.8	83.6	74.2	23.8	100	46.2	90.4	95.4	97.4	114.4	17.4	81.8	100	99.6	
Exp17	6.2	28.9	30.6	41.2	24.1	11.3	1.39	63.3	14.4	6.89	43.2	83.7	81.1	14.1	7.4	11.6	17.4	7.27	85.9	17	85.9	17	
Exp18	95.9	95.9	95.9	95.9	95.9	95.9	95.9	95.9	95.9	95.9	95.9	95.9	95.9	95.9	95.9	95.9	95.9	95.9	95.9	95.9	95.9	95.9	
Exp19	94.9	98.1	98.1	94.1	17.3	68.1	79.9	98.1	63.9	91.1	64.6	98.1	80.5	96.6	96.6	92.3	97.7	64.9	65.2	95.5	95.5	95.5	
Exp20	69.3	69.3	69.3	69.3	69.3	69.3	69.3	69.3	69.3	69.3	69.3	69.3	69.3	69.3	69.3	69.3	69.3	69.3	69.3	69.3	69.3	69.3	
Exp21	59	60.2	16.4	12.3	26.6	14.5	16.5	32.4	11.1	16.8	16.8	16.8	16.8	16.8	16.8	16.8	16.8	16.8	16.8	16.8	16.8	16.8	
Exp22	30.7	30.7	30.7	30.7	30.7	30.7	30.7	30.7	30.7	30.7	30.7	30.7	30.7	30.7	30.7	30.7	30.7	30.7	30.7	30.7	30.7	30.7	
Exp23	92	92	92	92	92	92	92	92	92	92	92	92	92	92	92	92	92	92	92	92	92	92	
Exp24	75.7	51.3	26.3																				

## References

1. Bertinetto, L., Valmadre, J., Golodetz, S., Miksik, O., Torr, P.H.S.: Staple: Complementary learners for real-time tracking. In: CVPR (2016) [6](#), [7](#)
2. Danelljan, M., Häger, G., Shahbaz Khan, F., Felsberg, M.: Accurate scale estimation for robust visual tracking. In: BMVC (2014) [6](#), [7](#)
3. Danelljan, M., Häger, G., Shahbaz Khan, F., Felsberg, M.: Convolutional features for correlation filter based visual tracking. In: ICCV Workshop (2015) [3](#), [6](#), [7](#)
4. Danelljan, M., Häger, G., Shahbaz Khan, F., Felsberg, M.: Learning spatially regularized correlation filters for visual tracking. In: ICCV (2015) [3](#), [6](#), [7](#)
5. Danelljan, M., Häger, G., Shahbaz Khan, F., Felsberg, M.: Adaptive decontamination of the training set: A unified formulation for discriminative visual tracking. In: CVPR (2016) [6](#), [7](#)
6. Danelljan, M., Robinson, A., Shahbaz Khan, F., Felsberg, M.: Beyond correlation filters: Learning continuous convolution operators for visual tracking. In: ECCV (2016) [1](#), [6](#), [7](#)
7. Danelljan, M., Shahbaz Khan, F., Felsberg, M., van de Weijer, J.: Adaptive color attributes for real-time visual tracking. In: CVPR (2014) [6](#), [7](#)
8. Felsberg, M.: Enhanced distribution field tracking using channel representations. In: ICCV Workshop (2013) [6](#), [7](#)
9. Galoogahi, H.K., Sim, T., Lucey, S.: Correlation filters with limited boundaries. In: CVPR (2015) [6](#), [7](#)
10. Gao, J., Ling, H., Hu, W., Xing, J.: Transfer learning based visual tracking with gaussian process regression. In: ECCV (2014) [6](#), [7](#)
11. Hare, S., Saffari, A., Torr, P.: Struck: Structured output tracking with kernels. In: ICCV (2011) [6](#), [7](#)
12. He, S., Yang, Q., Lau, R., Wang, J., Yang, M.H.: Visual tracking via locality sensitive histograms. In: CVPR (2013) [6](#), [7](#)
13. Henriques, J.F., Caseiro, R., Martins, P., Batista, J.: High-speed tracking with kernelized correlation filters. TPAMI 37(3), 583–596 (2015) [6](#), [7](#)
14. Jia, X., Lu, H., Yang, M.H.: Visual tracking via adaptive structural local sparse appearance model. In: CVPR (2012) [6](#), [7](#)
15. Kalal, Z., Matas, J., Mikolajczyk, K.: P-n learning: Bootstrapping binary classifiers by structural constraints. In: CVPR (2010) [6](#), [7](#)
16. Li, Y., Zhu, J.: A scale adaptive kernel correlation filter tracker with feature integration. In: ECCV Workshop (2014) [6](#), [7](#)
17. Liang, P., Blasch, E., Ling, H.: Encoding color information for visual tracking: Algorithms and benchmark. TIP 24(12), 5630–5644 (2015) [4](#), [7](#)
18. Ma, C., Huang, J.B., Yang, X., Yang, M.H.: Hierarchical convolutional features for visual tracking. In: ICCV (2015) [6](#), [7](#)
19. Ma, C., Yang, X., Zhang, C., Yang, M.H.: Long-term correlation tracking. In: CVPR (2015) [6](#), [7](#)
20. Nocedal, J., Wright, S.J.: Numerical Optimization. Springer, 2nd edn. (2006) [3](#)
21. Pinsky, M.: Introduction to Fourier Analysis and Wavelets. American Mathematical Society (2002) [1](#), [2](#)
22. Possegger, H., Mauthner, T., Bischof, H.: In defense of color-based model-free tracking. In: CVPR (2015) [6](#), [7](#)
23. Sevilla-Lara, L., Learned-Miller, E.G.: Distribution fields for tracking. In: CVPR (2012) [6](#), [7](#)



24. Szeliski, R.: Computer Vision: Algorithms and Applications. Springer-Verlag, 1st edn. (2010) [2](#)
25. Wu, Y., Lim, J., Yang, M.H.: Object tracking benchmark. TPAMI 37(9), 1834–1848 (2015) [4](#), [5](#), [6](#)
26. Zhang, J., Ma, S., Sclaroff, S.: MEEM: robust tracking via multiple experts using entropy minimization. In: ECCV (2014) [6](#), [7](#)